J. Fluid Mech. (1990), *vol.* 211, *pp.* 37–60
Printed in Great Britain

Vortex formation around an oscillating and translating airfoil at large incidences

By KAZUO OHMI[1], MADELEINE COUTANCEAU[2], TA PHUOC LOC[3] AND ANNIE DULIEU[3]

[1] Osaka University, Faculty of Language and Culture, Osaka 560, Japan
[2] Laboratoire de Mécanique des Fluides, Université de Poitiers, 86022 Poitiers Cedex, France
[3] Laboratoire d'Informatique pour la Mécanique et les Sciences de l'Ingénieur, 91403 Orsay Cedex, France

(Received 27 February 1989 and in revised form 10 July 1989)

The starting flows past a two-dimensional oscillating and translating airfoil are investigated by visualization experiments and numerical calculations. The airfoil, elliptic in cross-section, is set in motion impulsively and subjected simultaneously to a steady translation and a harmonic oscillation in pitch. The incidence of the airfoil is variable between 0° and 45° and the Reynolds number based on the chord length is between 1500 and 10000. The main object of the present study is to reveal some marked characteristics of the unsteady vortices produced from the oscillating airfoil set at large incidences in excess of the static stall angle. Another purpose is to examine, in some detail, the respective and combined effects of the major experimental parameters on the vortex wake development. It is shown that, in general, the dominant parameter of the flow is the reduced frequency not only when the airfoil oscillates at incidences close to the static stall angle but also at larger incidences. It is also demonstrated that, as the pitching frequency is increased, the patterns of the vortex wake are dependent on the product of the reduced frequency and the amplitude rather than on the frequency itself. It is noted that the combined effect of a high reduced frequency and a large amplitude can give rise to cyclic superposition of leading-edge vortices from which a gradually expanding standing vortex is developed on the upper surface.

1. Introduction

One of the most fundamental problems investigated in the domain of unsteady airfoils is the case in which the effective incidence of the airfoil oscillates periodically and accordingly the aerodynamic load fluctuates. This leads, in most cases, to generation of keen noises and marked vibrations of the airfoil body. In actual engineering situations, the oscillation of the incidence is caused usually by a periodic fluctuation of the external flow or by a forced oscillation of the airfoil itself. A typical example of the former is an airplane passing through turbulence, and of the latter is the pitching oscillation of a helicopter's main rotor; both are related to a number of important engineering problems.

Traditionally the research on this subject has often been oriented towards the critical flows in which the incidence oscillates close to the static stall angle but the recent development in aircraft technology and turbomachines increases the importance of the airfoils oscillating at large incidences as well. This kind of flow, often called 'deep dynamic stall' by aerodynamic engineers, has been investigated by

some experimenters (e.g. Werlé 1976 by extensive water channel experiments and Carr, McAlister & McCroskey 1977 by detailed wind tunnel experiments) and theorists (e.g. Ham 1968 by a discrete vortex approximation, Mehta 1977 by finite-difference calculations and Geissler 1985 by a panel method); these findings have been summarized by McCroskey (1977, 1982). However, most of them concern measured data representing flutuating load and/or static pressure, and the flow phenomena relative to these aerodynamic quantities remain to be analysed more closely. In addition a large number of experimental parameters, which often cause the complexity of the problem, are not always taken into account equally, that is, the researchers include usually only a few variable parameters in their analysis. So a comprehensive investigation of the problem is still lacking.

The present authors have tried therefore to conduct a systematic study, by visualization experiments and numerical calculations, on a two-dimensional oscillating airfoil in the starting flow regime. The study aims at revealing the phenomenology of the time-dependent processes in which a quasi-potential intitial wake develops into a definitely stalled flow. The discussion on these processes is chiefly from the viewpoint of vortex formation around the two edges and the subsequent development of vortical wakes. Most of the major experimental parameters are treated as variables and their respective and combined effects on the wake are investigated in detail. Some numerical calculations are carried out in parallel on the same oscillating model and the results are compared with the corresponding visualizations.

The airfoil with which we are concerned in the present paper is elliptic in cross-section and is subjected simultaneously to an impulsively started translating motion and a harmonic oscillation in pitch around the axis situated at mid-chord. We analyse the evolution of the wakes in their velocity fields and examine the effects of the oscillating frequency, the Reynolds number, the mean incidence and of the angular amplitude. The values of the angular parameters are so determined that the instantaneous incidence of the airfoil may go up to 45°, which is much in excess of the static stall angle of about 22°. The frequency of oscillation, which more or less exceeds the natural vortex-shedding frequency from a corresponding stationary airfoil, is given rather large values compared to most of the previously reported experiments and the consequent circumferential speed of the two edges is, at maximum, 1.6 times as large as the translating flow velocity. On the other hand, our Reynolds numbers, which are smaller than 10000, are not likely to produce shock waves or other compressible effects, so that the Mach number is excluded from our consideration.

2. Experimental set-up

The principle of the experiment is analogous to the one previously described by Coutanceau & Bouard (1977*a*, *b*), Bouard & Coutanceau (1980) and Coutanceau & Ménard (1985). However the set-up has been completely reconstructed, in particular it has been automated, significantly enlarged and oscillation generation added.

The visualization experiments are conducted in a tall rectangular water tank ($80 \times 100 \times 150$ cm^3) equipped with a vertical carrier movable in parallel. The principle of this apparatus, which can be considered as a variation of so-called towing tanks, consists in generating flows by means of vertical translation of the cylindrical body in still water, as is shown in figure 1. In this figure the model airfoil under water, the model support with the upper truss, the pitching generator and the photographic

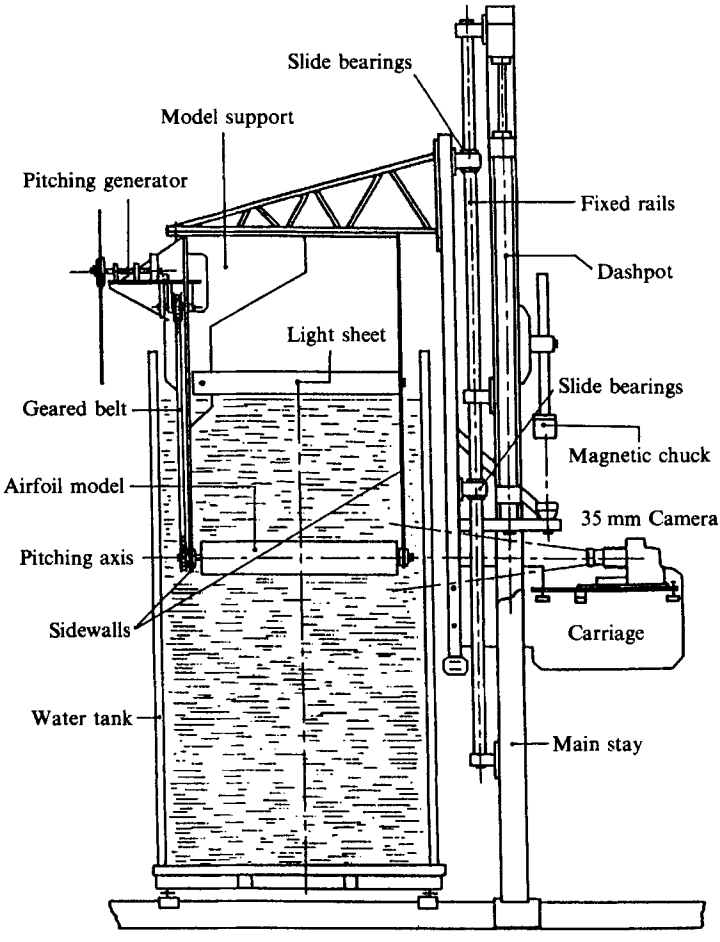

FIGURE 1. Apparatus for the flow visualization experiment.

stage attached to the inner frame are all connected in a body and descend vertically at a constant speed in the equilibrium of the gravity force with the dashpot damping force. This corresponds to the translation of the airfoil. The pitching oscillation of the airfoil is generated by a high-precision mechanical drive, the structural outline of which is illustrated in figure 2. This device transforms the vertical translation of the movable frame into a corresponding sinusoidal oscillation of the airfoil around the pitching axis. The pitching frequency is proportional to the speed of translation and therefore variable, but the reduced frequency is constant for a given chord length. When it is necessary to change the reduced frequency, the radius of the pulley is changed. The visualization, for the most part, is carried out by a pathline method using fine solid tracers, but in some cases it is aided by the additional use of a streakline method utilizing electrochemical tracers.

Two model airfoils are tested in the experiments; both are made of Plexiglas pieces and 60 cm in span. They are of a similar elliptic cross-section with 1/10 relative thickness, but one is 7 cm in chord and the other 14 cm. The choice between these two models depends mainly on the Reynolds number desired. The solid tracers used here are white Rilsan particles, which are irregularly crystalline, of about 80 to 200 μm major length. They are suspended in water uniformly after several

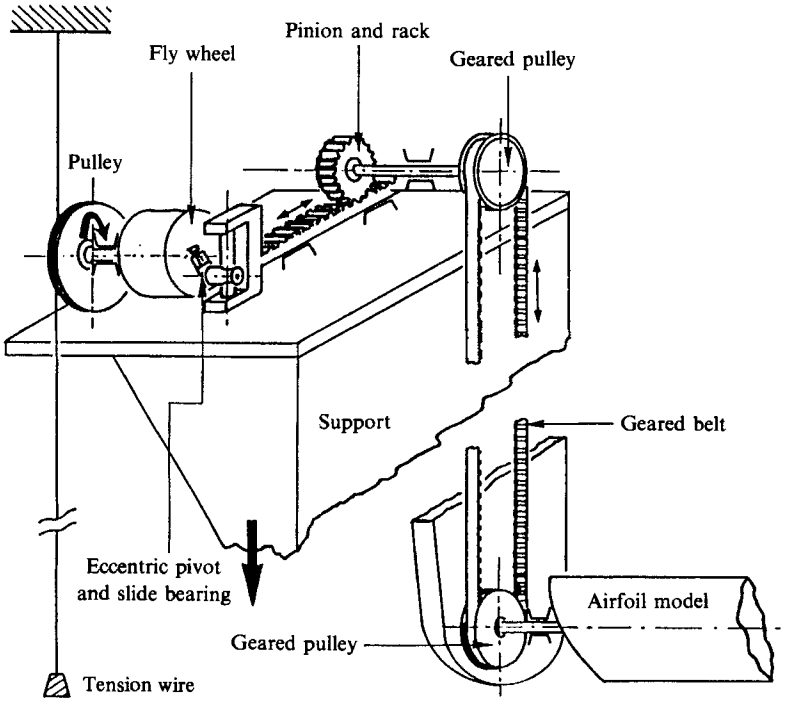

FIGURE 2. Pitching generator.

preselections and decantations. The electrochemical tracers are white precipitations of hydrated tin issued from the positive electrode in water. This electrode is a ring-style thin film of the metal attached onto the airfoil surface. The illumination is given by a sheet of intense light of 8 mm thickness, which cuts the flow in one of the middle cross-sections of the tank perpendicular to the span of the airfoil. A motor-driven 35 mm camera is fixed on the photographic stage in the direction parallel to the span and takes some 20 sequential frames from each experimental run, demonstrating the evolution of the starting flow. The visualization of pathlines by this camera corresponds therefore to that of quasi-instantaneous streamlines in the relative frame accompanying the airfoil translation but not the oscillation. The visual field of the camera is about 3 to 4 chords in width and 2–3 chords in height inclusive of the airfoil itself. A typical example of our pathline visualizations is presented in figure 3, where the airfoil is undergoing a rapid oscillation in pitch.

The startup of the model airfoil, performed by cutting off the current supplied to the electromagnetic chuck, is nearly impulsive but it takes finite time to attain the final descending speed. In most cases this time depends on the final speed itself and, according to our regular measurements on the larger model at $Re = 3000$, the initial translating speed attains 95% of the final speed after a displacement of 2 mm and 98.5% after a 4 mm displacement. As far as the effect of the model aspect ratio is concerned, we checked it frequently, at $Re = 3000$, by comparing two equivalent sequences of visualizations derived from our two model airfoils of aspect ratio 4.3 and 8.6 respectively. We have discovered as a result that the effect of this parameter is very small within the visual field of the photography, except for some time delay (of about 0.2 if expressed by the reduced time mentioned below) in the wakes of the smaller model. Since the chord length of the two models is different by a factor of two

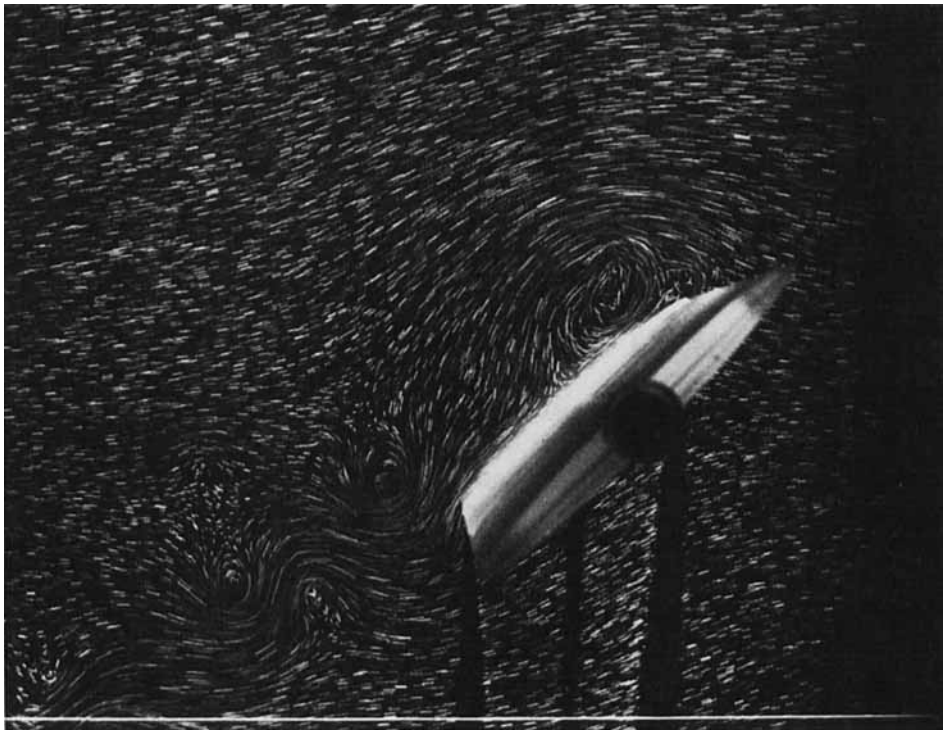

FIGURE 3. Visualization of a rapidly oscillating elliptic airfoil in an impulsively generated parallel flow; $Re = 3000$, $f^* = 1.0$, $\bar{\alpha} = 30°$, $\Delta\alpha = 15°$, $\alpha_0 = 15°$, $t^* = 1.25$.

and, therefore, their blockage ratio relative to the sidewalls and their duration of run expressed by the reduced time differ to the same extent, it is deduced from the above check experiments that the so-called wall effect and bottom effect are of little importance within the limits of our observations.

The numerical experiments are carried out on the basis of a finite-difference approximation of the unsteady two-dimensional Navier–Stokes equations. In order to accomplish the calculation for the Reynolds numbers up to 10^4 within a realistic computing time, we have developed a new algorithm making a combined use of the fourth-order and second-order compact Hermitian methods. The calculation results are presented in the form of streamlines in the same moving frame as in the visualization experiments. The details of this finite-difference algorithm are reported by Ta Phuoc & Daube (1980) and by Mane, Ta Phuoc & Werlé (1987).

In order that the effects of the major parameters can be closely examined, they are varied as follows

Reynolds number	$Re \equiv \dfrac{U_\infty c}{\nu} = 1500,\ 3000 \text{ or } 10000$
reduced frequency	$f^* \equiv \dfrac{fc}{2U_\infty} = 0.1,\ 0.5 \text{ or } 1.0,$
mean incidence	$\bar{\alpha} = 30° \text{ or } 15°,$
angular amplitude	$\Delta\alpha = 15° \text{ or } 7°,$
initial incidence	$\alpha_0 = \bar{\alpha} - \Delta\alpha \quad \text{or} \quad \bar{\alpha} + \Delta\alpha,$

where c is the chord of the airfoil, U_∞ the free-stream velocity at infinity or the

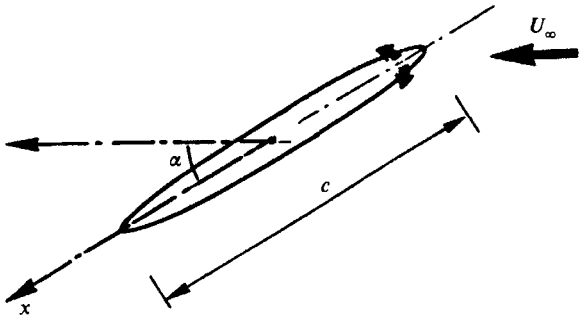

FIGURE 4. Coordinate system of the experiment.

translating speed and ν the kinetic viscosity of the fluid. Using some of these parameters, the coordinate system of our visualization experiments is illustrated in figure 4. There is no special reason why only the frequency is normalized by the half-chord length: it is merely because this normalization is more often employed in the existing literature. As regards the time-dependent oscillating motion of the airfoil, the instantaneous incidence α (t) is given by

$$\alpha(t) = \bar{\alpha} \pm \Delta\alpha \cos(2\pi f t) \quad \text{or} \quad \alpha(t^*) = \bar{\alpha} \pm \Delta\alpha \cos(4\pi f^* t^*).$$

Because of some technical restrictions, the flow observation is limited to the reduced time $t^* = 5.0$ $(t^* = tU_\infty/c)$ in most of the experiments. Therefore, the number of oscillation cycles experienced by the larger model within this limit is 1 if $f^* = 0.1$, 5 if $f^* = 0.5$ or 10 if $f^* = 1.0$.

There are a few experimental parameters which are not considered in the present study, such as the position of the pitching axis and the profile of the airfoil cross-section. Among these, the profile of cross-section may affect the separating flow significantly at the trailing edge, because most practical airfoils have a sharp trailing edge, in contrast to the rounded edge of the elliptic airfoil and, consequently, this may yield different separation conditions at the edge. The examination of these factors is scheduled in the next step of the research and the results will be published before long. The choice of an elliptic airfoil in the present paper is mainly because we are able to refer to some of the calculations by Lugt & Ohring (1977) and to predict the critical range of parameters to some extent. This choice is also related to the relative simplicity of the calculations without conformal mapping.

3. Analysis of the wakes

3.1. *Effect of reduced frequency*

From some of the existing literature on oscillating airfoils and our own test experiments, we have presumed that the predominant factor in our experiments is the reduced frequency f^*. So in the following wake analysis, the discussion is centred upon this parameter and, in order that the effect of f^* is demonstrated distinctly, a reference case is established among our numerous visualizations: the larger elliptic airfoil translating and oscillating at $Re = 3000$, $\bar{\alpha} = 30°$, $\Delta\alpha = 15°$ and $\alpha_0 = 15°$. The Reynolds number of 3000 was chosen because at this value the wake observation is little affected by turbulence, yet the generated wakes develop sufficiently that the time-dependent process of dynamic stall can be followed satisfactorily within the

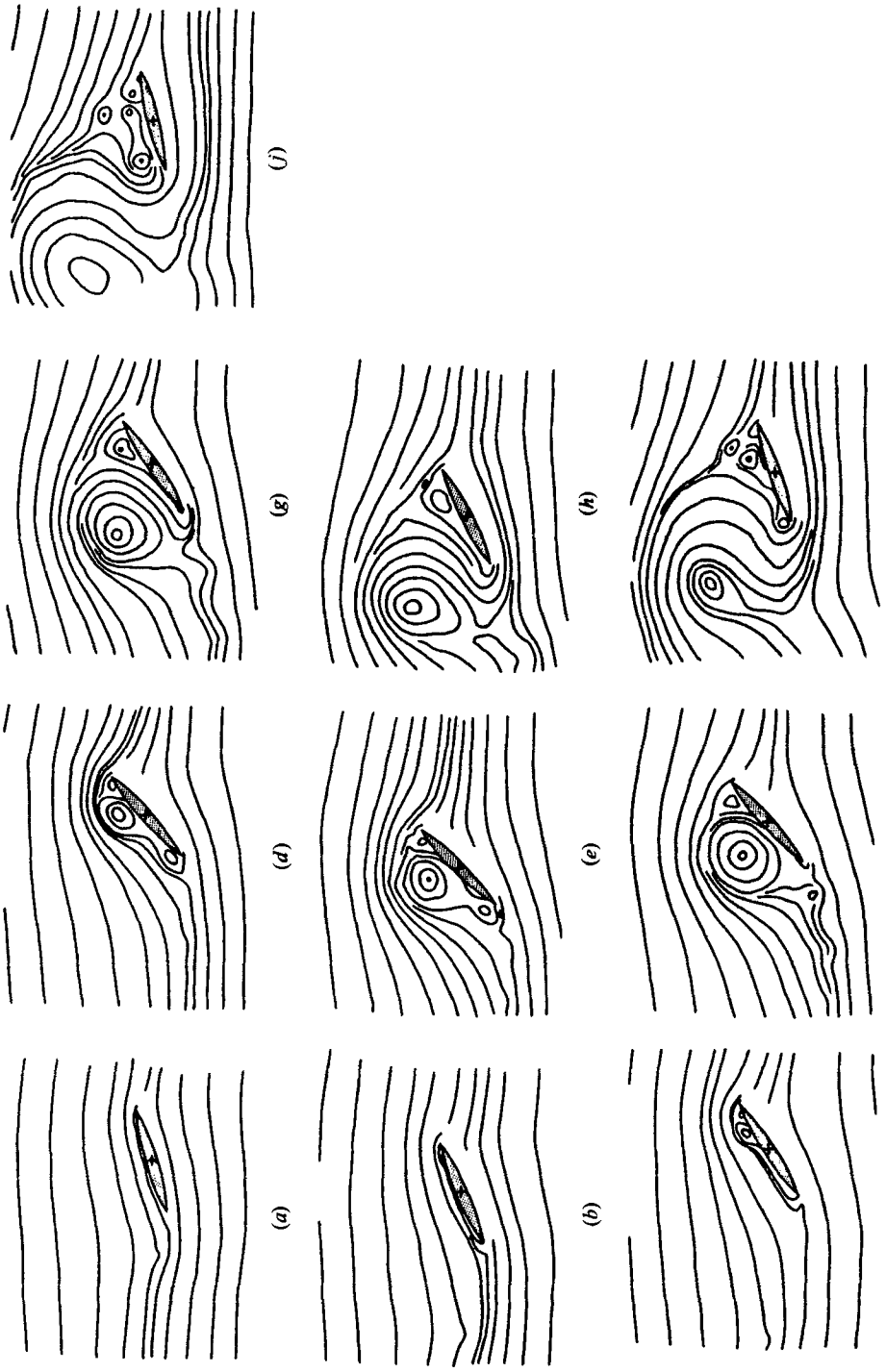

FIGURE 5. Sequence of streamline sketches derived from the visualization experiment at $f^* = 0.1$ ($Re = 3000$, $\bar{\alpha} = 30°$, $\Delta\alpha = 15°$, $\alpha_0 = 15°$): (*a*) $t^* = 0.5$, $\alpha_{(\mathrm{inst})} = 17.9°$; (*b*) 1.0, 25.4°; (*c*) 1.5, 34.6°; (*d*) 2.0, 42.1°; (*e*) 2.5, 45.0°; (*f*) 3.0, 42.1°; (*g*) 3.5, 34.6°; (*h*) 4.0, 25.4°; (*i*) 4.5, 17.9°; (*j*) 5.0, 15.0°.

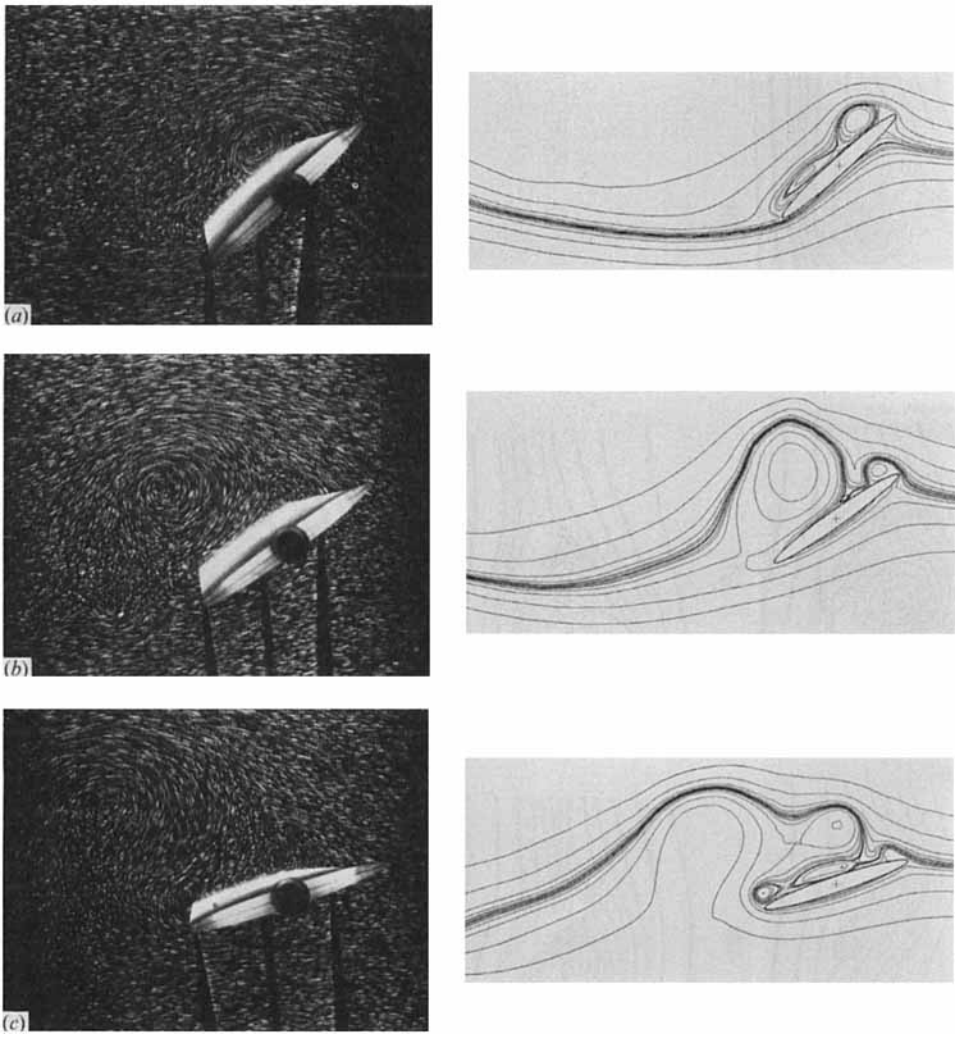

FIGURE 6. Selected comparisons between the experimental and numerical visualizations at $f^* = 0.1$ (left: experiment; right: calculation): (*a*) $t^* = 2.0$, $\alpha_{(\text{inst})} = 42.1°$; (*b*) 3.5, 34.6°; (*c*) 4.5, 17.9°.

experimental run. Each of the angular parameters is given the larger value because the characteristic features of the 'deep stall' regime are revealed more clearly.

3.1.1. $f^* = 0.1$

The streamline profiles observed in the starting flow visualization at $f^* = 0.1$ are sketched in figure 5, and figure 6 presents three of the original photographic frames selected from figure 5, together with the corresponding numerical calculations. The comparison between experiment and calculation shows that the correspondence is satisfactory until the end of the first half-cycle. Afterwards there arises some phase delay in the calculation but both flows are phenomenologically identical.

The starting flows at this frequency, in general, preserve the fundamental characteristics of the static stall experienced by a high-incidence fixed airfoil. After the detachment of the starting vortex (existing in the visual field until $t^* = 1.5$), the initial separation bubble develops into a large-scale leading-edge vortex spread all

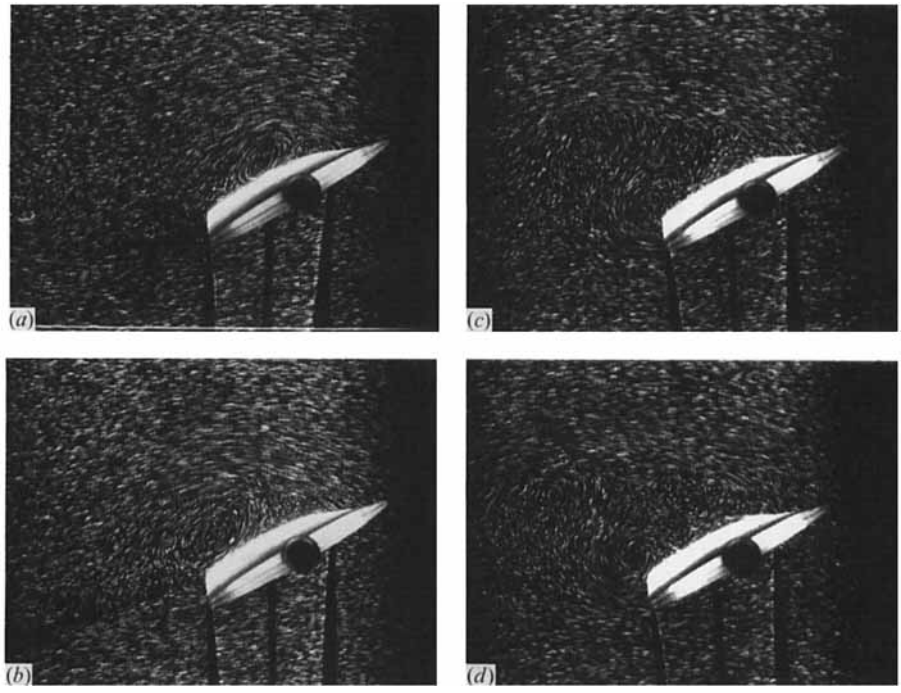

FIGURE 7. Visualization of a fixed elliptic airfoil ($Re = 3000$, $\alpha = 30°$): (*a*) $t^* = 1.5$, (*b*) 2.5, (*c*) 3.5, (*d*) 4.0.

over the upper surface ($t^* < 3.0$). This vortex detaches slowly from the airfoil while it draws up the lower-surface separating flow from behind the trailing edge ($t^* < 4.0$). The neighbouring streamlines then form a characteristic pattern representing an inverted S-shape ($t^* = 4.5$) and in the lower part of this inverted S a smaller trailing-edge vortex arises ($t^* = 5.0$). The analogy of this flow evolution with that of the static stall is easily recognized if our supplementary visualizations of a fixed airfoil given in figure 7 ($\alpha = 30°$, $Re = 3000$) are referred to. It is clear from the comparison with figure 5 that, in spite of some chronological differences in the vortex development, the initial wakes of the oscillating and the fixed airfoils have much in common. As regards the effect of the fixed incidence in this comparison, the experimental and numerical visualizations reported by Daube *et al.* (1985) and by Palmer & Freymuth (1984) serve for our reference. Evidently, from a number of comparisons, a fixed incidence in excess of the critical stall angle does not influence the initial wakes from the viewpoint of the phenomenology of vortices. It is concluded therefore that the oscillating airfoil at $f^* = 0.1$ generates vortical wakes primarily by the action of the translating flow and that the rotating motion of the airfoil produces rather secondary effects such as acceleration or deceleration of the vortex development.

However, this description does not imply that the response is quasi-steady at this reduced frequency. It is evident that the flow response to a given incidence is somewhat delayed on an oscillating model if compared to a corresponding fixed model. A chronological comparison between figures 6 and 7 shows that the flow evolution of the oscillating airfoil at $t^* = 2.0$, for instance, is approximately equivalent to that of the fixed airfoil at $t^* = 1.5$. Since the instantaneous incidence of the oscillating model is at an angle of 30° between $t^* = 1.0$ and $t^* = 1.5$ and goes

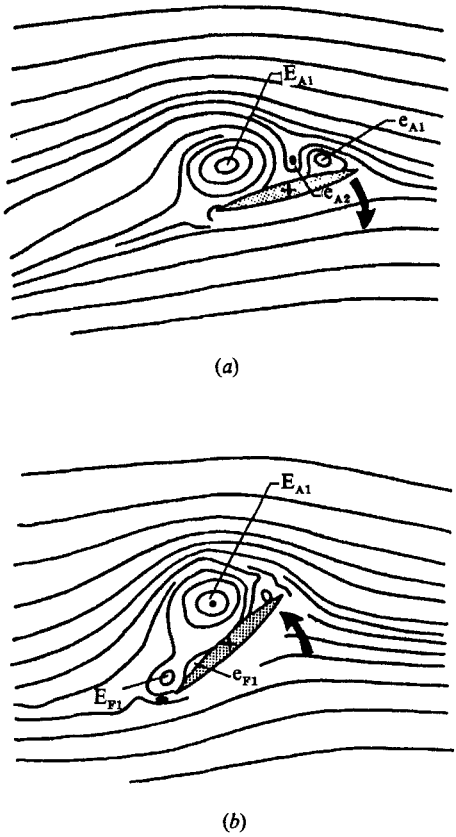

FIGURE 8. Leading-edge transverse motion and the relevant vortex motions in the flows oscillating at $f^* = 0.1$: (*a*) descent of the leading edge ($Re = 3000$, $\bar{\alpha} = 30°$, $\Delta\alpha = 15°$, $\alpha_0 = 45°$, $t^* = 2.0$, $\alpha_{(\mathrm{inst})} = 17.9°$); (*b*) ascent of the leading edge ($Re = 3000$, $\bar{\alpha} = 30°$, $\Delta\alpha = 15°$, $\alpha_0 = 15°$, $t^* = 2.5$, $\alpha_{(\mathrm{inst})} = 45°$).

up to 42.1° when $t^* = 2.0$, the delay of response on this latter model is all the more convincing.

The effect of airfoil rotation is recognizable in the relation between the leading-edge transverse motions and the subsequent behaviour of the relevant vortices. The point is illustrated by two of the representative visualization frames of figure 5, which are reproduced with comments in figure 8. Obviously the descent of the leading edge (figure 8*a*) restrains the leading-edge separation, because of comparatively rapid adjustment of the separating flow to the incidence decrease, and stops further development of the leading-edge vortex E_{A1}, while giving rise to a secondary vortex e_{A1} at the front of the upper surface and promoting the detachment of the main part E_{A1}. On the other hand, the ascent of the leading edge (figure 8*b*) consolidates the leading-edge separation and favours stable development of the leading-edge vortex E_{A1}, while in the rear part of the upper surface a pair of secondary vortices, E_{F1} and e_{F1}, are generated under the influence of the trailing-edge descent. Both of these observations are indicative that the translating flow around the airfoil is still capable of adjusting to the time variation of incidence and that the wake, as a whole, remains within the static stall regime. Further evidence for this explanation is provided by the visualization experiments attempted by Werlé (1976) on a NACA 0012 airfoil

oscillating in pitch at mid-chord ($Re = 12000, f^* = 0.15, \bar{\alpha} = 20°, \Delta\alpha = 20°, \alpha_0 = 0°$). It is evident, from some of the visualization sequences covering two cycles of oscillation, that the development rate of the leading-edge vortices is more important during the ascending phase than during the descending phase.

Since the larger airfoil model at this frequency completes only one cycle of oscillation during the experimental run, some comments are added on the second cycle, based only on the visualization of the smaller model. We conclude that the flow evolution of the second cycle is not very different from that of the first cycle despite the influence of the starting process. The initial stage of the second cycle is dominated by the trailing-edge vortex which is definitely formed at $t^* = 5.0$ and shed rather rapidly thereafter ($t^* = 6.0$). Meanwhile, the leading-edge separating flow approaches the upper surface after the detachment of the residual part of the previous leading-edge vortex (equivalent to e_{A1} in figure 8*a*). However, the moment that the oscillating incidence exceeds 30° again ($t^* = 6.5$), a new leading-edge vortex starts to be formed at the front of the edge and another cycle analogous to the preceding one is repeated until $t^* = 10.0$. The whole cycle is shortened a little and, therefore, the development of the alternate vortices is less important, but there are hardly any specific phenomena which are observable only in the second cycle.

3.1.2. $f^* = 0.5$

The streamline sketches of the visualization experiment at $f^* = 0.5$ are shown in figure 9 and the comparative presentation of the experimental and numerical results is given in figure 10. In this last figure, the correspondence is satisfactory until the end of the third cycle but, afterwards, the detachment and the downstream motion of the leading-edge vortices are progressively decelerated in the calculation. However, the periodic nature of the vortices is more or less maintained.

One remarkable feature of the flows at this frequency is that the rotating motion of the airfoil plays an important role in the establishment of vortical wakes, that is to say, the periodic vortex formation here is primarily due to the fluid reaction, or the inertia, against the transverse motions of the two edges. So, differently from the preceding case, the descent of the leading edge ($t^* = 1.0, 2.0...$) favours rapid development of the leading-edge vortices and the ascent ($t^* = 1.5, 2.5...$) tends towards the suspension of further development of the leading-edge vortices. Concerning the trailing-edge motions, on the other hand, the rapid oscillation gives rise to cyclic alternate vortices, the rotation of which is in the opposite sense to that of the trailing edge. In addition, the starting vortex is merged into the first trailing-edge vortex produced by the downstroke and both are visually inseparable. All of these observations are closely related to the growing importance of the rotation effect on the vortex wake development. Among the alternate vortices generated from the trailing edge, however, those formed by the upstroke of the edge are comparatively weakened owing to the undisturbed translating flow coming from the lower surface.

Further evidence of the dominant rotation effect at this frequency is provided by the leading-edge counter-rotating vortices formed at the front of the lower surface during every upstroke of the edge. These counter-rotating vortices are generally small and their formation is rather momentary during the upstroke, so that it is somewhat difficult to recognize them in the pathline visualizations by solid tracers. But they are distinctly observable in the streakline visualizations using electrochemical tracers, which are given in figure 11. In this figure, all the streaks representative of counter-rotating vortices (indicated by white arrows) are generated during the preceding upstroke of the edge, move towards the upper surface in the

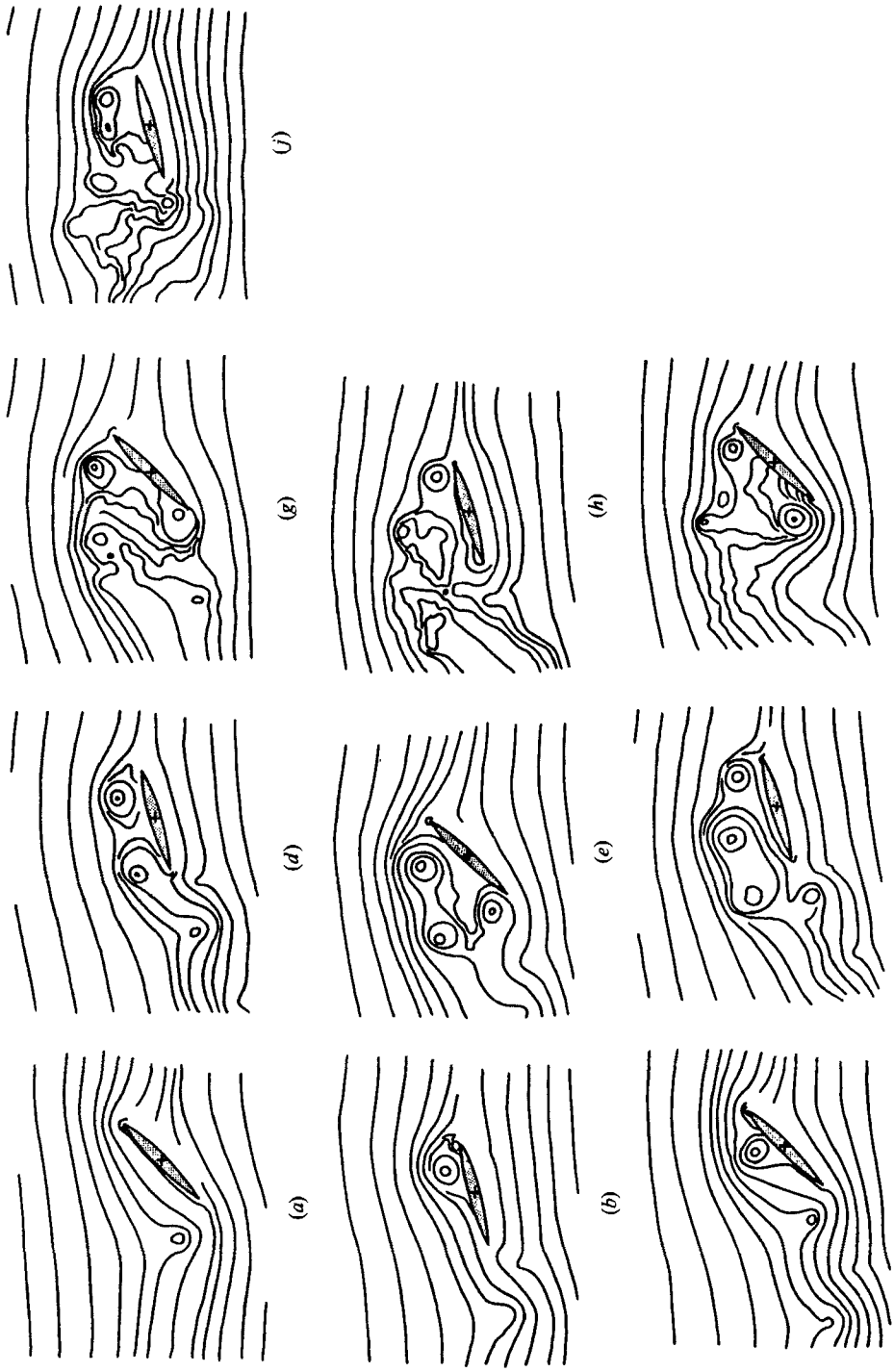

FIGURE 9. Sequence of streamline sketches derived from the visualization experiment at $f^* = 0.5$ ($Re = 3000$, $\bar{\alpha} = 30°$, $\Delta\alpha = 15°$, $\alpha_0 = 15°$): (*a*) $t^* = 0.5$, $\alpha_{(inst)} = 45.0°$; (*b*) 1.0, 15.0°; (*c*) 1.5, 45.0°; (*d*) 2.0, 15.0°; (*e*) 2.5, 45.0°; (*f*) 3.0, 15.0°; (*g*) 3.5, 45.0°; (*h*) 4.0, 15.0°; (*i*) 4.5, 45.0°; (*j*) 5.0, 15.0°.

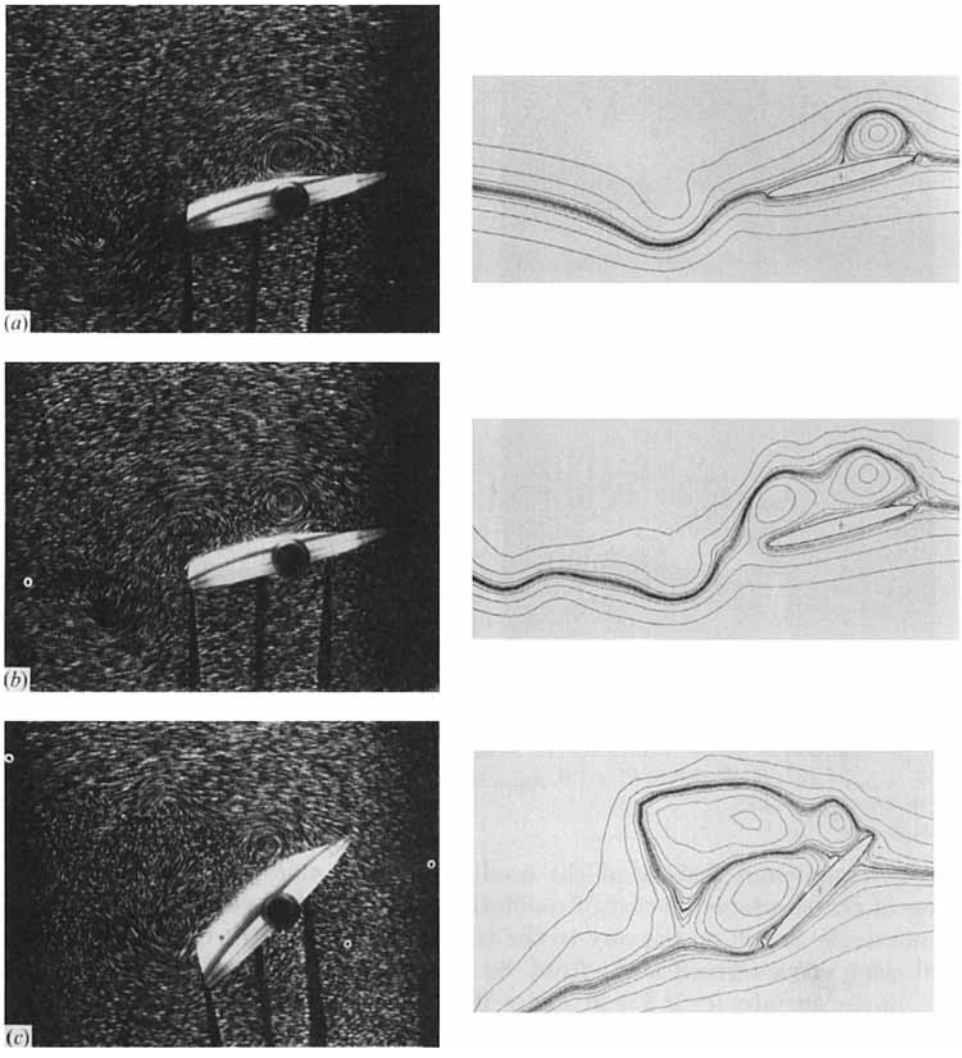

FIGURE 10. Selected comparisons between the experimental and numerical visualizations at $f^* = 0.5$ (left: experiment; right: calculation): (*a*) $t^* = 1.0$, $\alpha_{(\text{inst})} = 15°$; (*b*) 2.0, 15°; (*c*) 4.5, 45°.

following downstroke and, then, coupled with the major upper-surface vortices. It should be noted here that the existence of these counter-rotating vortices is indicative of the fact that the backward-moving speed of the leading-edge surface, induced by the increase in incidence, exceeds momentarily the downstream velocity of the boundary layer around this edge and, consequently, the separation is oriented towards the lower-surface side with respect to the stagnation point. There has been some mention by experimenters of the leading-edge counter-rotating vortices, such as Walker & Helin (1985), Gad-el-Hak (1986) and Gad-el-Hak & Ho (1986), but it appears that they are referring to the secondary vortices generated *within* the upper-surface major vortex, equivalent in our experiments to e_{A2} in figure 8(*a*), and nothing is said about the direction of the leading-edge separating flow. This is probably because the recognizable production of the counter-rotating vortices of this type depends on the shape of the leading edge and the pitching axis.

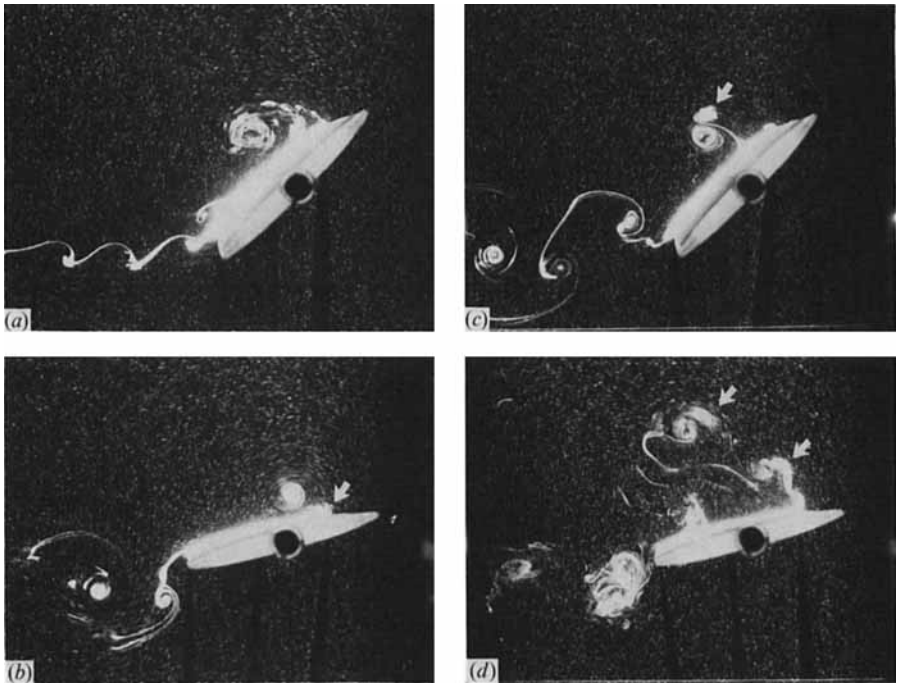

FIGURE 11. Streakline visualizations of the flows past an oscillating airfoil; the experimental parameters common to all the frames are: $Re = 3000$, $\bar{\alpha} = 30°$, $\Delta\alpha = 15°$ and $\alpha_0 = 15°$. (*a*) $f^* = 0.1$, $t^* = 2.5$, $\alpha_{(\text{inst})} = 45°$; (*b*) $f^* = 0.5$, $t^* = 1.0$, $\alpha_{(\text{inst})} = 15°$; (*c*) $f^* = 0.5$, $t^* = 1.5$, $\alpha_{(\text{inst})} = 45°$; (*d*) $f^* = 0.5$, $t^* = 4.0$, $\alpha_{(\text{inst})} = 15°$.

Another important feature of the oscillating flows at $f^* = 0.5$ is the fact that, because of the shortened period of oscillation, every leading-edge vortex formed in the downstroke is still on the way to the trailing edge along the upper surface when the following one is formed at the front. So at least two vortices exist simultaneously on the upper surface ($t^* \geqslant 2.0$ in figure 9) and their number increases with time ($t^* \geqslant 4.0$). This is partly because the travelling speed of the vortices is reduced owing to the suction effect from the rapidly descending leading-edge surface and partly because these vortices, on arrival at the trailing edge, gradually fail to be shed in synchronization with the periodic vortices of the trailing edge itself. Therefore the leading-edge vortices start to behave independently of the trailing-edge ones, detach from the airfoil midway on the upper surface and align approximately in parallel with the outer translating flow ($t^* \geqslant 3.5$). In consequence, a viscous region is spread all over the upper surface and the downstream motion of the shed vortices is decelerated furthermore ($t^* \geqslant 4.0$). The wake reaches finally an advanced stall regime, in which one observes two separation systems originating from the leading and the trailing edges.

3.1.3. $f^* = 1.0$

The streamline sketches from the visualization experiment at $f^* = 1.0$ are shown in figure 12 and the comparative visualizations for three selected frames are presented in figure 13. The correspondence between experiment and calculation is reasonable until the time $t^* = 3.0$.

The major point about the flows at this frequency is, as is the case for the

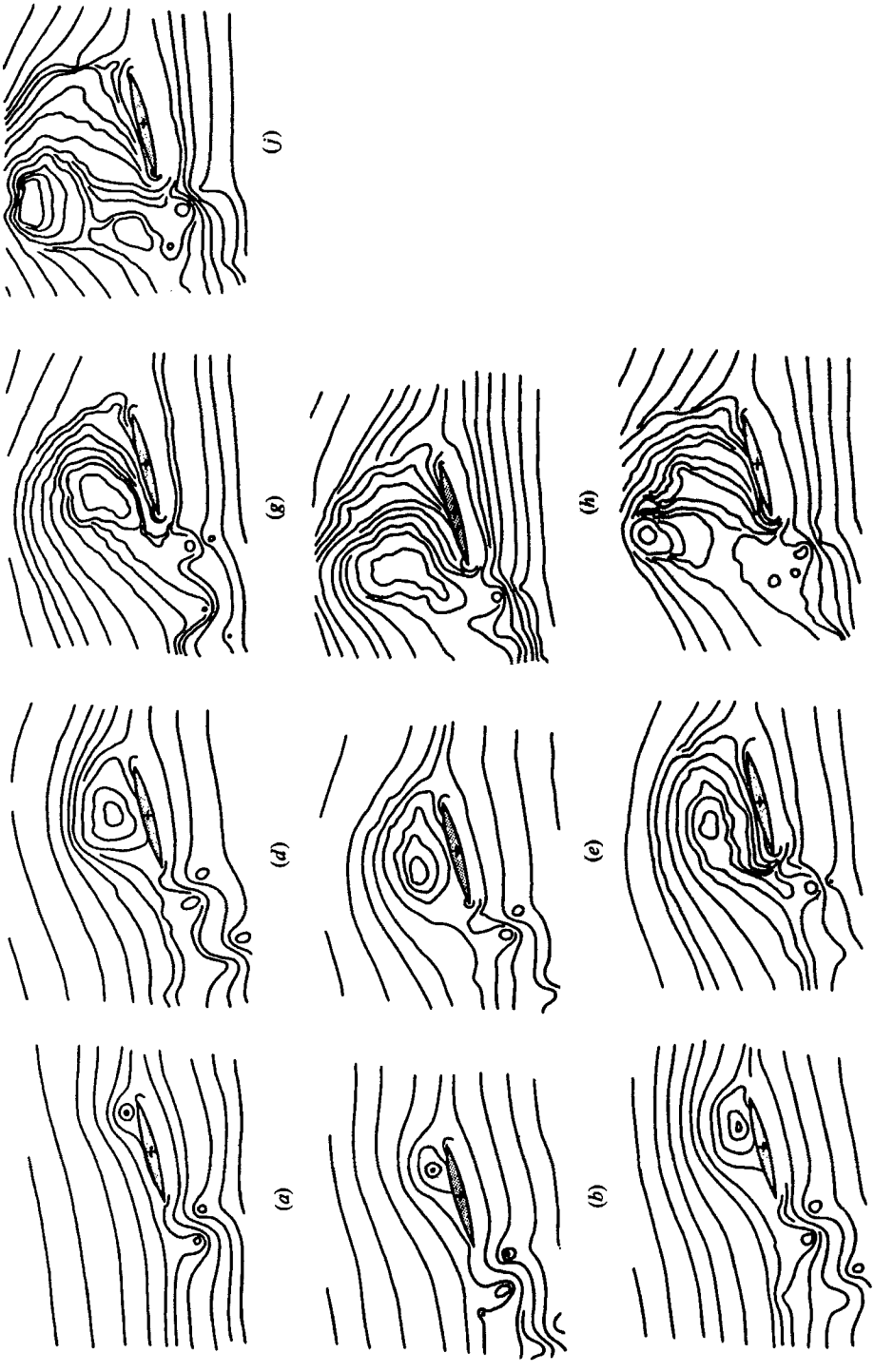

FIGURE 12. Sequence of streamline sketches derived from the visualization experiment at $f^* = 1.0$ ($Re = 3000$, $\bar{\alpha} = 30°$, $\Delta\alpha = 15°$, $\alpha_0 = 15°$): (*a*) $t^* = 0.5$, $\alpha_{(\mathrm{inst})} = 15.0°$; (*b*) 1.0, 15.0°; (*c*) 1.5, 15.0°; (*d*) 2.0, 15.0°; (*e*) 2.5, 15.0°; (*f*) 3.0, 15.0°; (*g*) 3.5, 15.0°; (*h*) 4.0, 15.0°; (*i*) 4.5, 15.0°; (*j*) 5.0, 15.0°.

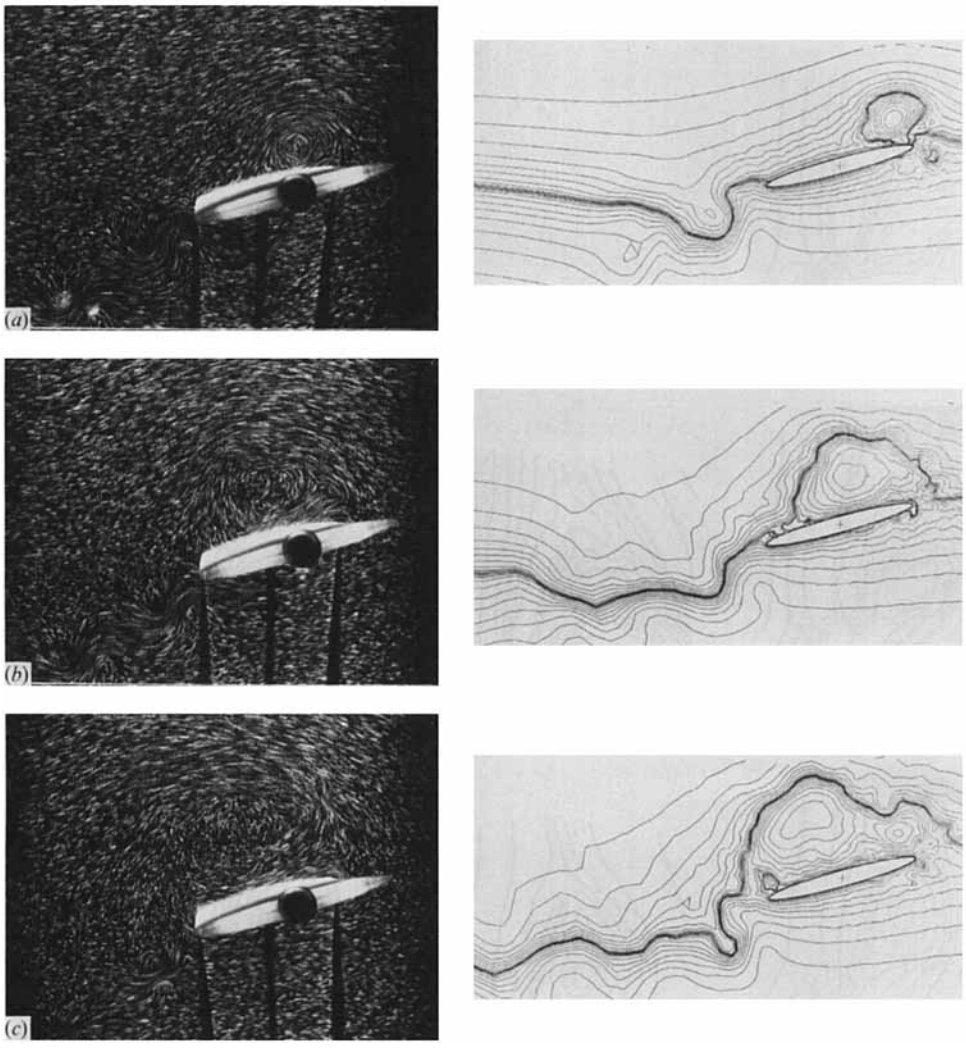

FIGURE 13. Selected comparisons between the experimental and numerical visualizations at $f^* = 1.0$ (left: experiment; right: calculation): (*a*) $t^* = 1.0$, $\alpha_{(\mathrm{inst})} = 15°$; (*b*) 2.0, 15°; (*c*) 3.0, 15°.

oscillation at $f^* = 0.5$, that the periodically generated vortices and the subsequent vortical wakes are primarily due to the fluid reaction against the rapid rotation of the airfoil. However, here, the transverse motions of the two edges are more violent, so that the leading-edge counter-rotating vortices, generated during the upstroke, are observable even in the pathline visualizations (cf. figure 3). In addition, the trailing-edge alternate vortices generated by the ascending and descending motions are almost of the same scale, which contributes to the formation of a well-balanced vortex street downstream, in the initial stages at least.

The most marked difference of the present flow from the preceding one at $f^* = 0.5$ consists in the dynamics of the leading-edge vortices after the periodic generation. Since the counterclockwise-rotating vortices, produced by every downstroke of the leading edge, hardly alter their positions relative to the airfoil even in the following upstroke, they are superposed on the upper surface from cycle to cycle and coalesce into a single standing vortex ($t^* \leqslant 2.0$). This standing vortex, increasingly supplied

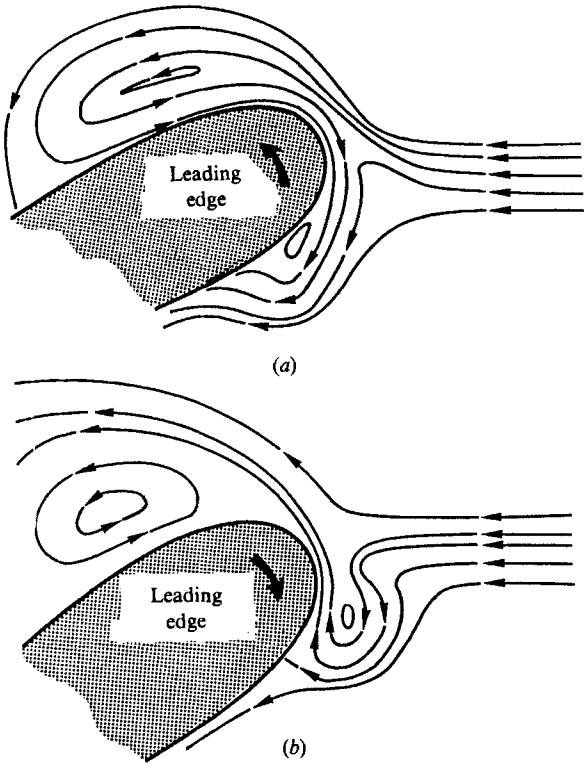

FIGURE 14. Conceptual illustrations of the relation between the leading-edge transverse motion and the relevant vortex motions at $f^* = 1.0$: (*a*) ascent of the leading edge, (*b*) descent of the leading edge.

with vorticity, is developed slowly until it covers the entire upper surface ($t^* = 2.5$). Then, it draws up the lower-surface separating flow from behind the trailing edge, forms a streamline pattern in an inverted S-shape ($3.0 \leqslant t^* \leqslant 4.0$) and gradually detaches from the airfoil while spreading in the direction perpendicular to the chord ($t^* = 5.0$). Because of this standing vortex, a permanent lift is expected on the obstacle. However, taking a general view of the flow, the development process of this standing vortex bears some analogy to that of the leading-edge vortex in the static stall regime.

The leading-edge vortices hardly alter their relative positions during the violent alternation of upstroke and downstroke, primarily because an important suction effect is produced by the rapidly descending upper surface. The downstream motion of the vortices is almost suppressed by this strong effect. In addition, the interaction effect is significant between the vortex pair generated at the front on the upper and lower surfaces. This last effect, schematically illustrated in figure 14, is explained as follows. A counterclockwise-rotating vortex is formed on the upper surface as a result of the leading-edge descent, part of the reverse flow within this vortex goes upstream beyond the front of the leading edge now in ascent, continues into the lower-surface flow separating from the ascending edge and rejoins the clockwise-rotating vortex developing there (figure 14*a*). This lower-surface vortex exercises an exactly opposite action upon the upper-surface flow when the leading edge re-enters the descending phase and the counterclockwise-rotating vortex is developed again on the upper

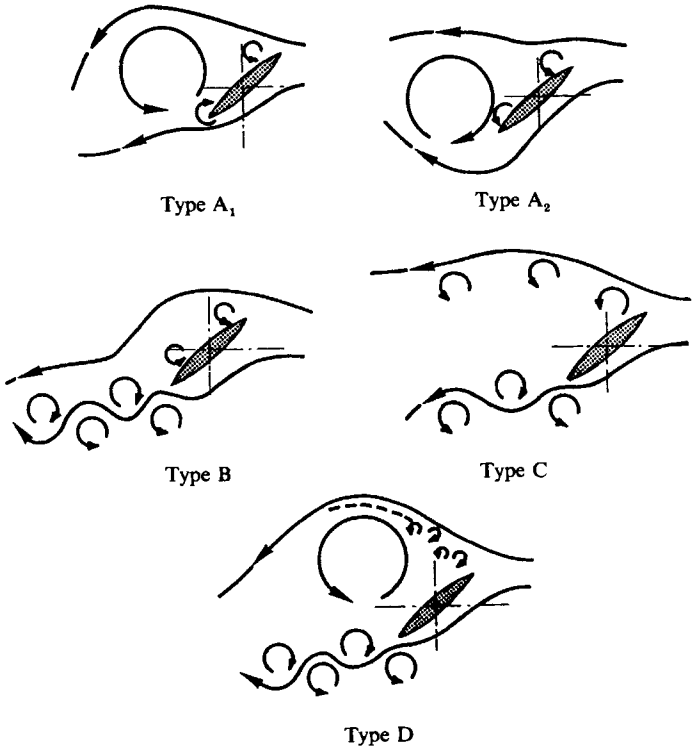

FIGURE 15. Classification of wake patterns.

surface (figure 14*b*). And reiterating this fluid-exchange process consisting of complicated alternation between inertial and viscous behaviour, the leading-edge vortex pair progressively associate with each other and, as a result, their relative positions are hardly altered in spite of the rapid oscillation of the airfoil.

On the other hand, the trailing-edge transverse motion is initially concerned with the regularly alternate vortex generation and shedding toward downstream ($t^* \leqslant 1.5$ in figure 13). But the moment that the leading-edge standing vortex is spread over the upper surface and the entire surface is covered with reverse flow ($t^* = 2.5$), the vortex formation during the upstroke (lower-surface vortices) starts to be restrained and that of the downstroke (upper-surface vortices) promoted. So the consequent vortex street loses the regularly alternate nature of the shed vortices and becomes rather symmetric with respect to the centerline of the wake ($t^* \geqslant 2.5$).

3.2. *Classification of wake patterns*

In the preceding section, we have fixed the values of three major parameters (Reynolds number Re, mean incidence $\bar{\alpha}$ and angular amplitude $\Delta\alpha$) with a view to a detailed discussion on the effects of the reduced frequency f^*. In this section, however, the three parameters are varied and their respective and combined effects on the wake generated are discussed. The first step is an overall analysis of the photographic frames representing the various wakes encountered in the experiments. The wakes analysed are classified in terms of their characteristic patterns as illustrated in figure 15. The classified wake patterns are then correlated with the experimental conditions in table 1, where the pattern notation corresponds to that

Angles			Frequency	Elliptic airfoil (mid-chord)		
$\bar{\alpha}$	$\Delta\alpha$	α_0	$f^* = fc/2U_\infty$	$Re = 1500$	$Re = 3000$	$Re = 10000$
30°	15°	45°	0.1	A	A	A
		15°		A	A	A
		45°	0.5	B→C	B→C	B→C
		15°		B→C	B→C	B→C
		45°	1.0	—	D	D
		15°		—	D	D
15°	15°	30°	0.1	A	A	A
		0°		A	A	A
		30°	0.5	B→C	B→C	B→C
		0°		B→C	B→C	B→C
		30°	1.0	—	D	D
		0°		—	D	D
30°	7°	37°	0.1	A	A	A
		23°		A	A	A
		37°	0.5	B→C	B→C	B→C
		23°		B→C	B→C	B→C
		37°	1.0	—	B→C	B→C
		23°		—	B→C	B→C
15°	7°	22°	0.1	A	A	A
		8°		A	A	A
		22°	0.5	B→BC	B→BC	B→BC
		8°		B→BC	B→BC	B→BC
		22°	1.0	—	B→BC	B→BC
		8°		—	B→BC	B→BC

TABLE 1. Variation of the wake patterns according to experimental conditions; the pattern notation corresponds to that of figure 15.

of figure 15. Within the classification of table 1, the difference of the starting vortices is not taken into account because these affect very little the subsequent wake development. The arrows connecting two pattern notations in table 1 indicate that the observed wake pattern evolves during the experimental run and some blanks signify the absence of the corresponding visualizations. The details of the classified patterns in figure 15 are explained as follows.

Type A: A starting flow similar to that of a high-incidence fixed airfoil. The leading-edge vortex, after being spread over the upper surface, detaches from the airfoil slowly while forming a characteristic streamline pattern in an inverted S-shape, the lower part of which develops into another trailing-edge vortex (called 'static stall type' hereafter). The two variant types, A_1 and A_2, represent different origins (leading or trailing edge) and different rotating senses of the dominant vortex observed during the first cycle, and depend on whether the initial incidence is maximum or minimum.

Type B: Every one of the leading-edge vortices, on arrival at the trailing edge along the upper surface, behaves in association with the periodic vortices of the trailing edge itself. More precisely, the leading-edge vortices are combined into the corotating trailing-edge vortices one by one and then shed downstream in a synchronized manner ('synchronized shedding type').

Type C: The leading-edge vortices travelling on the upper surface detach from the

airfoil without reaching the trailing edge and are shed downstream almost in parallel to the outer flow. Meanwhile, the trailing edge generates and sheds its own alternate vortices. As a result, there develop two parallel vortex-shedding systems, or two separation systems, originating from the leading and the trailing edges ('parallel shedding type').

Type BC: An intermediate pattern between Types B and C.

Type D: The leading-edge vortices, generated in every downstroke of the edge, are superposed one after another on the upper surface and coalesce into a single standing vortex. This standing vortex is developed slowly from cycle to cycle and detached gradually from the airfoil while spreading in the direction perpendicular to the chord ('vortex superposition type').

3.3. *Effect of mean incidence*

In order to examine the effects of this parameter, a comparative analysis has been made between pairs of sequences of visualization for which the experimental conditions are identical except for the mean incidence. Bearing in mind the pattern variations in table 1, the results of this analysis are summarized as follows.

3.3.1. *General remarks*

As the mean incidence $\bar{\alpha}$ is increased from 15° to 30°, the periodic vortices developing from the leading and the trailing edges gain in scale and the interaction between them is reduced. However, the fundamental features of the generated wake are not affected by the increase in $\bar{\alpha}$, whether the airfoil oscillates at incidences larger or smaller than the static stall angle.

3.3.2. $f^* = 0.1$

Independently of the angular amplitude $\Delta\alpha$, as the mean incidence $\bar{\alpha}$ is increased, the initial leading-edge vortex becomes more spread and stable and it remains longer in the vicinity of the airfoil. However, apart from the geometry of vortices, the effect of $\bar{\alpha}$ turns out to be small on the whole.

3.3.3. $f^* = 0.5$

In comparison with the preceding case where $f^* = 0.1$, the effect of $\bar{\alpha}$ is revealed a little more clearly. As is indicated by the pattern notation in table 1, most of the wake patterns at $\bar{\alpha} = 15°$ are of either the synchronized shedding or the parallel shedding type depending on the values of $\Delta\alpha$, while the patterns at $\bar{\alpha} = 30°$ always result in the parallel shedding type.

3.3.4. $f^* = 1.0$

As is shown in table 1, the effect of $\bar{\alpha}$ differs distinctly according to the amplitude $\Delta\alpha$. If $\Delta\alpha = 7°$, the wake patterns are varied from the parallel shedding to the vortex superposition type with increase in $\bar{\alpha}$, while if $\Delta\alpha = 15°$, they result in the vortex superposition type independently of $\bar{\alpha}$. So in the latter case, the effect of the mean incidence itself is not clear.

3.4. *Effect of angular amplitude*

The effect of this parameter is examined, as is in the preceding section, by comparing pairs of visualization sequences with different values of amplitude. The results of this examination are summarized as follows.

3.4.1. *General remarks*

As the angular amplitude is increased from 7° to 15°, every leading-edge vortex gains in scale and the consequent vortical wake is widened. However, from a general point of view, this effect of increase in $\Delta\alpha$ is not so important as that produced by increased $\bar{\alpha}$.

3.4.2. $f^* = 0.1$

As the angular amplitude is increased, the development of the leading-edge vortices is encouraged and their geometry is less disturbed even during the shedding process. And from the viewpoint of the scale of vortices, the variation of wake patterns with the amplitude $\Delta\alpha$ is nearly the same as that for the mean incidence $\bar{\alpha}$. But it is somewhat difficult to discuss further the effects of $\Delta\alpha$ itself, mainly because the variation of wake patterns is caused by that of both the amplitude and the mean incidence. Re-examining the visualization sequences in various combinations of $\Delta\alpha$ and $\bar{\alpha}$, it is deduced that the determinant factor of the wakes at this frequency is the maximal incidence $\alpha_{\max}$ rather than the respective angles of $\bar{\alpha}$ and $\Delta\alpha$. However, the difference of wake patterns in terms of this parameter is much less important than that classified in figure 15, and this reconfirms the preceding observation that the wake remains within the vicinity of the static stall regime.

3.4.3. $f^* = 0.5$

As far as the periodic vortices originating from the leading and trailing edges are concerned, the increase in $\Delta\alpha$ produces the same effects as those at the reduced frequency f^*. So the leading-edge counter-rotating vortices, for instance, are hardly observable if $\Delta\alpha = 7°$ whereas they are momentarily detectable if $\Delta\alpha = 15°$. At the same time, the ordinarily rotating (counterclockwise-rotating) vortices are subjected to a more significant suction effect from the descending leading-edge surface. Their downstream motion being decelerated recognizably, they stay longer in the vicinity of the oscillating airfoil. Therefore it is considered that the effects of $\Delta\alpha$ and of f^* are mutually compensatory with respect to the establishment of wake patterns.

3.4.4. $f^* = 1.0$

As is mentioned in §3.3.4, the vortex behaviour and the consequent wake patterns differ clearly according to the values of $\Delta\alpha$. Among the varied patterns observed at this frequency, those of the vortex superposition type at $\Delta\alpha = 15°$ are considered as a special case in which the rotation effect of the airfoil is prominent, and therefore separated from the other patterns at $\Delta\alpha = 7°$ or from the general patterns at $f^* = 0.5$. Within the wakes of last two cases, on the other hand, the mutually compensatory relation between $\Delta\alpha$ and f^*, mentioned in the preceding paragraph, is revealed more distinctly in table 1. If the correspondence between the wake patterns for $f^* = 1.0$ and for $f^* = 0.5$ is examined while keeping the mean incidence identical, it is seen that the patterns at $\Delta\alpha = 7°$ in the former correspond almost exactly to those at $\Delta\alpha = 15°$ in the latter. This correspondence of the patterns is generally seen also in our continued experiments on an oscillating NACA 0012 airfoil in more varied experimental conditions. It is concluded therefore that the determinant factor of the wake past a high-frequency oscillating airfoil is the product of the reduced frequency and the angular amplitude $f^*\Delta\alpha$, or the maximal pitching rate $(\partial\alpha/\partial t)_{max}$, rather than the frequency itself.

3.5. *Effect of Reynolds number*

This effect is examined by comparing sets of three series of visualizations at Re = 1500, 3000 and 10000 while keeping the other parameters identical. However, this comparison is limited to the last two Reynolds numbers at $f^* = 1.0$, because of the absence of the visualizations at $Re = 1500$. A summary of the comparative analysis is given below.

3.5.1. *General remarks*

As is suggested by the pattern variations in table 1, the fundamental processes of the periodic vortex formation and of the subsequent wake establishment are not affected by the variation of the Reynolds number. Nevertheless, there is a general tendency observable at every reduced frequency: the increase in Re often results in acceleration of the initial wake development and in reduction of the transitional phase existing between the initial and established wakes.

3.5.2. $f^* = 0.1$

With the increase in Re, the wake around the oscillating airfoil tends to adjust more promptly to the time variation of incidence. And this tendency is clearly recognizable in the visualization experiments at Re = 10000. In particular if $\bar{\alpha} = 15°$ *and* $\Delta\alpha = 7°$, the general aspects of the leading-edge separation are switched rapidly across an incidence of about 15° and, within this critical angle, the upper-surface flow passing over the leading edge becomes almost parallel to the airfoil surface and yield momentarily an apparently separationless regime. (Needless to say, the term 'separationless' excludes the separation near the trailing edge.) Another point at this frequency is that the increase in Re up to 10000 causes in most cases growing turbulence within the vortical wakes and affects the dynamics of small-scale fluid motions. When examining the starting flows with small angular parameters ($\bar{\alpha} = 15°$ *and* $\Delta\alpha = 7°$), for instance, the initial stage of the wake finds a couple of fine dispersive leading-edge bubbles travelling along the upper surface with short wavelengths. As regards the starting flows with the larger angular parameters ($\bar{\alpha} = 30°$ *and* $\Delta\alpha = 15°$), there are some recognizable effects of turbulence observable in the irregular fluctuation of the pathline directions inside the upper-surface vortices, which are still stable as a whole.

3.5.3. $f^* = 0.5$

In most of the starting flows at Re = 10000, as long as the angular parameters are small, the same tendency as described in §3.5.1 is detectable to some extent, that is to say, the leading-edge separating flow is switched rapidly according to the time variation of incidence. But from a general point of view, the final wake patterns at this frequency result in either the synchronized shedding or the parallel shedding type depending upon the values of $\bar{\alpha}$ and $\Delta\alpha$ for the most part, the effect of Re on the pattern determination being much less important. The major effect of increased Re is the acceleration in establishing these wake patterns.

3.5.4. $f^* = 1.0$

The general observations mentioned above in §3.5.3 are still valid as long as $\Delta\alpha = 7°$, though, in most of the starting flows at Re = 10000, the marked development of the leading-edge and trailing-edge counter-rotating vortices complicates the downstream evolution of the wakes. In comparison, in the case $\Delta\alpha = 15°$, where the

wake patterns always result in the vortex superposition type, the local perturbation observed within the superposed leading-edge vortex is rather reduced at $Re = 10000$. At this Reynolds number, the development and the shedding of the trailing-edge vortices are also more stable and more regularly alternate. So the periodicity of the downstream wake is preserved for longer.

4. Conclusions

We have investigated, in detail, the starting flows past a high-incidence elliptic airfoil oscillating in pitch at mid-chord. Some difficulty has been encountered in the analysis of a mass of visualization frames which are nevertheless well classified. The first point is the distinction of physically independent factors from dependent ones in the course of the parametric analysis. The effects of each experimental parameter are not necessarily analysable from a single comparison of the relevant visualization sequences, but it is always necessary to take account of other parameters which may depend, directly or indirectly, on the parameter in question. Another point is the fact that the wake establishment at the lower frequencies is often influenced by the transient flows existing in the intermediate stages and that the chronology of the wakes can be varied by the smallest change in the experimental environment. So we are obliged to check often the reproductability of our experiments. In spite of these difficulties, we have attempted to draw conclusions which we think are free from physical ambiguity. The results of this attempt are the following:

(1) The general aspects of the starting flow past an oscillating airfoil are changed rather dramatically with increase in the reduced frequency. In our experiments, the critical frequency of this change is between $f^* = 0.1$ and 0.5

(2) In the case of the oscillating flows at $f^* = 0.1$, the generation of the vortex wake is primarily due to the translating flow, similarly to the case of a fixed airfoil, and the pitching rotation of the airfoil produces rather secondary effects, such as acceleration or deceleration of the vortex development. In other words, the generated wake remains within the static stall regime.

(3) In contrast, in the case of the oscillating flows at $f^* = 0.5$ or 1.0, the vortex wake generation is attributed mainly to the rotation of the airfoil or, more precisely, it is the fluid reaction or the inertia against the violent transverse motions of the two edges that plays a principal role in the production of periodic vortices.

(4) In the latter case where $f^* = 0.5$ or 1.0, the wake patterns are subdivided in terms of the vortex motions relative to the airfoil oscillation. The determinant factor of this subdivision is the product of the reduced frequency and the angular amplitude $f^*\Delta\alpha$ rather than the frequency itself.

(5) If the estimated value of $f^*\Delta\alpha$ is 0.26 (product of 1.0 and 0.26 rad) or more, the effect of the airfoil rotation becomes prominent and is concentrated upon the surrounding fluid. In consequence, all the wake patterns that result are of the vortex superposition type, in which the periodic leading-edge vortices are superposed from cycle to cycle and coalesce into a single standing vortex on the upper surface.

(6) On the other hand, if the estimated value of $f^*\Delta\alpha$ is 0.12 (product of 1.0 and 0.12 rad) or less, the periodically generated upper-surface vortices, originating from the leading and the trailing edges, are shed downstream with more or less interaction. And the final wake patterns differ to some extent, mainly according to the mean incidence $\bar{\alpha}$.

(7) In the last case where $f^*\Delta\alpha \leqslant 0.12$, if the main incidence $\bar{\alpha}$ is below the critical stall angle, the wake patterns result in the alternative of the synchronized shedding

or the parallel shedding type, whereas if $\bar{\alpha}$ is much in excess of the critical angle, the resultant wake patterns are always of or close to the parallel shedding type.

(8) As far as the fundamental dynamcis of vortices and the general aspects of wakes are concerned, the effect of the Reynolds number is much less important than that of the other parameters.

This study is supported by the Direction des Recherches, Études et Techniques of France under a contract entitled 'Unsteady Wakes'. The Laboratoire de Mécanique des Fluides, Université de Poitiers is associated to the CNRS under the U.R.A. 191.

REFERENCES

BOUARD, R. & COUTANCEAU, M. 1980 The early stages of development of the wake behind an impulsively started cylinder for $40 < Re < 10^4$. *J. Fluid Mech.* **101**, 583–607.

CARR, L. W., MCALISTER, K. W. & MCCROSKEY, W. J. 1977 Analysis of the development of dynamic stall based on oscillating airfoil experiments. *NASA Tech. Note* D-8382.

COUTANCEAU, M. & BOUARD, R. 1977*a* Experimental determination of the main features of the viscous flow in the wake of a circular cylinder in uniform translation. Part 1. Steady flow. *J. Fluid Mech.* **79**, 231–256.

COUTANCEAU, M. & BOUARD, R. 1977*b* Experimental determination of the main features of the viscous flow in the wake of a circular cylinder in uniform translation. Part 2. Unsteady flow. *J. Fluid Mech.* **79**, 257–272.

COUTANCEAU, M. & MENARD, C. 1985 Influence of rotation on the near-wake development behind an impulsively started circular cylinder. *J. Fluid Mech.* **158**, 399–446.

DAUBE, O., TA PHUOC, L., MONNET, P. & COUTANCEAU, M. 1985 Ecoulement instationnaire décollé d'un fluide incompressible autour d'un profil: une comparaison théorie-expérience. *AGARD Conf. Paper* 386, Paper 3.

GAD-EL-HAK, M. 1986 The use of the dye-layer technique for unsteady flow visualization. *Trans. ASME J. Fluids Engng* **108**, 34–38.

GAD-EL-HAK, M. & HO, C-M. 1986 Unsteady vortical flow around three-dimensional lifting surfaces. *AIAA J.* **24**, 714–721.

GEISSLER, W. 1985 Unsteady boundary-layer separation on airfoils performing large-amplitude oscillations – dynamic stall. *AGARD Conf. Paper* **386**, Paper 7.

HAM, N. D. 1968 Aerodynamic loading on a two-dimensional airfoil during the dynamic stall. *AIAA J.* **6**, 1927–1934.

LUGT, H. J. & OHRING, S. 1977 Rotating elliptic cylinders in a viscous fluid at rest or in a parallel stream. *J. Fluid Mech.* **79**, 127–156.

MCCROSKEY, W. J. 1977 Some current research in unsteady fluid dynamics – The 1976 Freeman Scholar Lecture. *Trans. ASME* I: *J. Fluids Engng* **99**, 8–39.

MCCROSKEY, W. J. 1982 Unsteady airfoils. *Ann. Rev. Fluid Mech.* **14**, 285–311.

MANE, L., TA PHUOC, L. & WERLÉ, H. 1987 Sur le décollement instationnaire autour d'un profil à grands nombres de Reynolds: une comparaison calcul expérience. *C. R. Acad. Sci. Paris*, II **305**, 229–232.

MEHTA, U. B. 1977 Dynamic stall of an oscillating airfoil. *AGARD Conf. Paper* **227**, Paper 23.

PALMER, M. & FREYMUTH, P. 1984 Analysis of vortex development from visualization of accelerating flow around an airfoil starting from rest. *AIAA Paper* 84–1568.

TA PHUOC, L. & DAUBE, O. 1980 Higher order numerical solution of unsteady viscous flow generated by a transversely oscillating elliptic cylinder. *Winter Annual Meeting ASME* (Book No. G00181), 155–171.

WALKER, J. M. & HELIN, H. E. 1985 An experimental investigation of an airfoil undergoing large amplitude pitching motions. *AIAA Paper* 85-0039.

WERLÉ, H. 1976 Visualisation hydrodynamique de l'écoulement autour d'une pale oscillante. *ONERA Rapp. Tech.* 56/1369.